

## Turbulent combustion of biomass syngas

K. KWIATKOWSKI, K. BAJER, K. WĘDOŁOWSKI

*Faculty of Physics  
University of Warsaw  
Pasteura 7  
02-093 Warsaw, Poland  
email: kamil@igf.fuw.edu.pl  
and  
Interdisciplinary Centre for Mathematical  
and Computational Modelling  
University of Warsaw*

BIOMASS SYNGAS, A LOW-CALORIFIC GAS continuously produced in the process of biomass pyrolysis and gasification, a relatively little-known fuel, can be used for heat production in an industrial plant. However, stringent emission norms have to be fulfilled at all times. In this paper, we present numerical simulations of turbulent combustion of the biomass syngas. They show that strict norms can be kept and that the process does not need any additional oil-burners to sustain the mandatory temperature. We have created a 3D model of the real industrial syngas combustion chamber of complex geometry involving an axial co-flow jet and six additional air inlets to enhance the swirl and to promote the generation of vortices. We have run a series of non-premixed combustion simulations for the syngases produced from wood chips and from turkey feathers.

**Key words:** biomass syngas, biomass gasification, turbulent combustion, CFD.

Copyright © 2012 by IPPT PAN

### Notations

$C_d$	dissipation constant,
$D$	molecular diffusion coefficient,
$\tilde{k}$	Favre-averaged turbulent kinetic energy,
$N$	scalar dissipation rate,
$Sc$	turbulent Schmidt number,
$u_k$	$k$ -component of the velocity vector,
$Y_\alpha$	mass fraction of the specie $\alpha$ ,
$\tilde{\epsilon}$	Favre-averaged energy dissipation,
$\nu_{\text{turb}}$	turbulent viscosity,
$\xi$	mixture fraction,
$\bar{\phi}$	mean value (in sense of Reynolds averaging) of the quantity $\phi$ ,
$\tilde{\phi}$	mean value (in sense of density-weighted averaging) of the quantity $\phi$ ,

---

This work has been presented at the 19th Polish National Fluid Dynamics Conference, Poznań 2010.

- $\phi'$  fluctuation of  $\phi$  from the Reynolds averaged value,
- $\phi''$  fluctuation of  $\phi$  from the density-weighted averaged value,
- $\phi_{st}$  value of quantity  $\phi$  where the mixture fraction equals its stoichiometric value,
- $\omega_\alpha$  production term of the specie  $\alpha$ .

## 1. Introduction

GASIFICATION APPEARS TO BE THE MOST ECONOMICALLY promising way of thermal treatment of the solid biomass waste [11, 18, 10]. An in-house industrial installation enables clean waste disposal, which would otherwise require costly outside contracting, and, in the simplest version, generates heat used in the plant's technological process. The combination of the two benefits makes even the simplest gasifier-combustor-boiler systems commercially viable provided the process is carefully designed to be clean enough, so that the composition of the flue gases meets the environmental norms ([1, 2]) and the cost of their additional purification is limited. Electric power co-generation can considerably improve the economy of the whole process but any efficient co-generation, whether with a gas turbine or internal combustion engine, requires much bigger initial investment in a system of syngas cleaning.

All three components of the gasifier-combustor-boiler system must be individually designed for different types of solid biomass waste. Of those three, it is the combustor which has the main effect on the composition of the flue gases. It has to be individually designed for the target flow rate and for the particular syngas composition determined by the kind of biomass fed into the gasifier [8]. Some of the pollutants present in the flue gases are robust. Their content is determined by the chemical composition of waste biomass and they have to be removed from the flue gases by the specific chemical treatment. This is the case, for example, with sulphur for which stable and reliable removal processes are known and ready desulphurisation installations are available. Other pollutants are highly sensitive to the details of the combustion process and their concentration in the flue gases may vary by more than one order of magnitude depending on the apparently small change in the design of the combustion chamber, burner, oxidant supply configuration, etc. This is the case with the  $\text{NO}_x$  which are extremely sensitive to the details of the reacting flow inside the combustion chamber [9, 6]. Their concentration measured in the flue gases may vary greatly without any noticeable change in the control parameters of the industrial process [14].

To somewhat lesser extent this is also the case with carbon monoxide (CO). Its chemistry is more robust and predictable than that of the  $\text{NO}_x$  but its emission may be affected by possible irregular dynamics of the flow causing puffs of unburned CO to exit the combustion chamber from time to time. A straightforward countermeasure would be to raise the temperature of the combustion

process but this is antagonistic to the reduction of the  $\text{NO}_x$ . Another limit on lowering temperature is the requirement imposed on the combustion of syngas originating from waste material. Such syngas and all exhaust gases must be subject to temperature no less than  $850^\circ\text{C}$  for at least 2 seconds ([1, 2]). This requirement has to be ensured by an additional oil burner, which, in case of temperature decrease, has to be switched on automatically. Since changing temperature in the combustion chamber is restricted by such opposing environmental constraints the question arises whether these conditions are possible to fulfil in industrial devices.

In the present work we focus on two different kinds of low-calorific biomass syngases, the first produced during the gasification of wood chips, the second produced during the gasification of poultry feathers. We show, using numerical simulations, that even such low-calorific gases can be burnt in an industrial combustion chamber without any additional burners, with pollutant emissions comfortably below the legal emission limits.

## 2. Materials

### 2.1. The biomass syngas

The process of biomass gasification produces a unique combustible gas called biomass syngas. This fuel is fully renewable and contains mainly nitrogen (unless gasification was done in pure oxygen and biomass was nitrogen-free when nitrogen would be absent), hydrogen and carbon monoxide. Detailed compositions are shown as mass fractions in Table 1. The compositions of these syngases

**Table 1. Composition (mass fraction) of biomass syngases produced in the gasification of wood chips [8] and turkey feathers [7].**

Notation	reference syngas <sup>1)</sup>	wood syngas	wood syngas	feather syngas	feather syngas
	RS	WS1	WS2	FS1	FS2
Nitrogen	0.568	0.567	0.583	0.549	0.599
Carbon Mono.	0.281	0.268	0.280	0.030	0.068
Hydrogen	0.015	0.006	0.005	0.005	0.003
Carbon Di.	0.110	0.096	0.071	0.396	0.299
Oxygen	0.005	0.023	0.025	0.000	0.014
Water	0.000	0.014	0.014	no data	no data
Methane	0.020	0.019	0.015	0.020	0.015
Ethane	0.000	0.001	0.001	no data	no data
Propane	0.000	0.005	0.005	no data	no data
LHV [MJ/kg]	5.65	4.66	4.46	1.91	1.80

<sup>1)</sup> Biomass syngas. Source: [www.treepower.org](http://www.treepower.org).

were measured in two industrial gasification plant: the first, located in Szepietowo [8], utilising wood chips; the second, located in Olsztyn, close to a poultry slaughterhouse [7, 14], utilising turkey feathers.

Due to its relatively low mean calorific value, strongly fluctuating composition and admixture of soot and other solid components, the syngas is most often burnt in combustion chambers. More advanced applications, like for example using syngas as fuel for the IC engines, are in their infancy. The syngas contains methane and other hydrocarbons, so in order to perform proper modelling of combustion in a chamber the scheme for chemical reactions must go beyond the combustion of only hydrogen and CO ([9]) and include hydrocarbons.

The syngas generally contains only trace amounts of hydrocarbons with more than three atoms of carbon (Table 1). The energy contained in  $C_2H_6$  and  $C_3H_8$  is around 6% of the total chemical energy of wood-derived syngases. Hence, we can use the GRI3 [19] detailed mechanism of chemical reactions and thermodynamic data for reaction calculations. It is based on 6 elements and 53 species appropriate for syngas and includes more than 300 reactions.

## 2.2. Syngas combustion

Combustion of biomass syngas differs from combustion of other gaseous fuels. Gasifiers, especially fixed-bed, produce low-calorific gases at the temperature around 1000 K [7]. In the combustion chamber these hot fuels are mixed with cold air. The stoichiometric value is typically close to 0.5, i.e., the proportion of air and gas is close to one.

Environmental regulations require that the combusting gases spend no less than 2 seconds in the region of high temperature (minimum 850 °C). For a given gas volume flux at the inlet, determined by the production rate of the gasifier, this imposes a lower bound on the volume of the combustion chamber, which in the installation we are modelling is about 36 m<sup>3</sup>. In such a large-scale industrial syngas device turbulence occurs naturally. The estimated values of the Reynolds number spanning the range of flows in our simulations of the non-reactive case, i.e. ‘cold’ flow, are of the order of 10<sup>5</sup>. Hence, the flow is clearly turbulent and turbulence modelling must be used. The highest value of the Reynolds number, based on the diameter of the fuel inlet and on the fuel inlet velocity, is equal  $1.87 \times 10^5$ .

A sketch of the simulated combustion chamber is presented in Fig. 1. It consists of a vertical cylinder with a system of fuel and air inlets installed in the top surface and an outlet located near the bottom of the cylindrical side wall. The position of the outlet in the wall makes for a major departure from axial symmetry. The axial (vertical) cross-section which includes the centre of the outlet pipe is denoted ( $x$ - $z$ ) plane. Another asymmetry is due to the additional

swirl-enhancing air inlets in the top surface. Symmetrically placed on a circle concentric with the main axial jet those alone would make only small, possibly negligible, departure from axial symmetry. However, due to the combination of discrete auxiliary inlets at the top and the fixed position of the outlet, the system has neither planar nor axial symmetry.

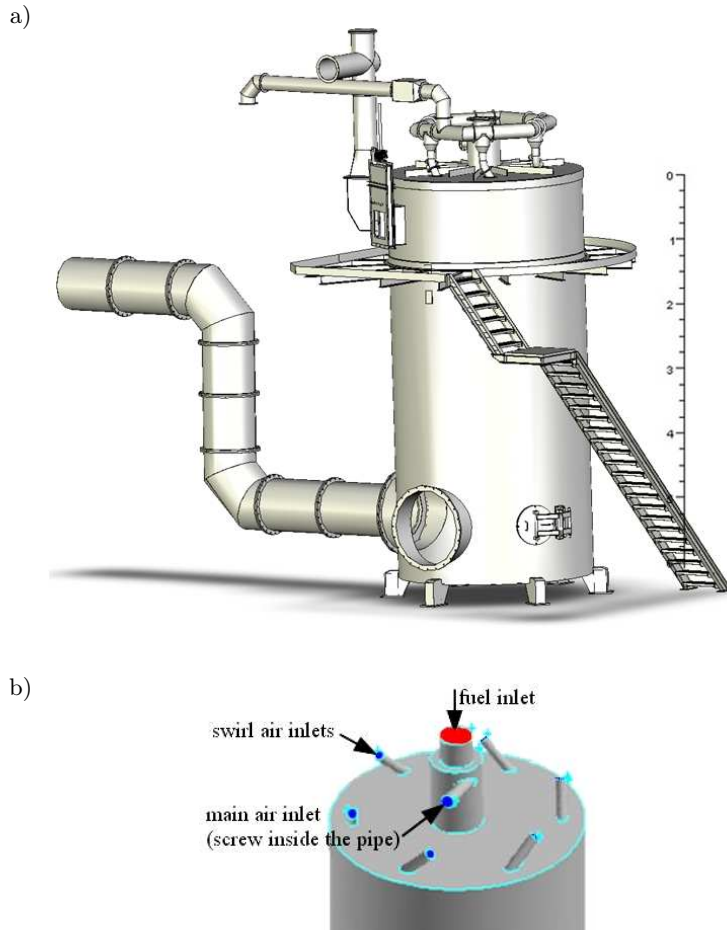


FIG. 1. The 3D model of the syngas burner. Six additional inclined inlet pipes mounted in the top wall induce swirl. Details of the inlets are presented in the lower picture.

In our simulations the values of the gas and air inlet velocities correspond to the typical values measured in the industrial devices (particularly in the industrial installation for thermal waste conversion in operation in Olsztyn). The boundary conditions are explained in Fig. 1. The values of the boundary conditions are listed in Table 2. Since the cold flow simulations include no chemical

**Table 2. Boundary conditions for turbulent non-premixed combustion.**

Boundary	$V_{\text{axial}}$ [m/s]	$V_{\text{radial}}$ [m/s]	$V_{\text{swirl}}$ [m/s]	$\xi$ [-]	$\xi'^2$ [-]	$T_{\text{emp}}$ [K]
Fuel inlet	10	0	0	1	0	800
Main air inlet	2	0	3	0	0	300
Swirl air inlets	6	0	6	0	0	300
Walls	0	0	0	0	0	1000

reactions, and the density of the syngases is comparable with the density of air, we assume air as the working fluid for both the oxidiser inlets and for the fuel inlet.

### 3. Methods

#### 3.1. Conserved scalar approach

All species present in the combustion chamber obey the advection-diffusion equation with the nonlinear source terms describing the chemical conversions of the species.

Under the assumption of equal diffusivities of all species – a reasonable assumption for turbulent flow, we can use the conserved scalar approach to separate the modelling of the flow from that of combustion [4]. For turbulent, non-premixed combustion it is convenient to introduce the mixture fraction variable,  $\xi$  (sometimes denoted by  $f$ ), defined at every instant over the whole domain, to be the mass fraction of the material that originated from the fuel stream. The origin of the material is an invariant during the chemical reactions, so the mixture fraction is conserved (Eq. (3.1)).

$$(3.1) \quad \frac{\partial(\rho\xi)}{\partial t} + \frac{\partial(\rho u_k \xi)}{\partial x_k} = \frac{\partial}{\partial x_k} \left( \rho D \frac{\partial \xi}{\partial x_k} \right).$$

If combustion does not occur, the mixture fraction simplifies to the fuel mass fraction.

We usually normalise mixture fraction, so that  $\xi = 1$  in the fuel stream and  $\xi = 0$  in the oxidiser stream which simplifies the boundary conditions for fuel and oxidiser inlets (see Table 2). Mass fractions of the particular species of fuel are presented in Table 1. The sum over all species should be 1.

For large-scale complex flows with turbulence the conservation equation (also Eq. (3.1)) has to be averaged.

The Favre-averaged version of the equation of mixture fraction conservation takes the following form:

$$(3.2) \quad \frac{\partial(\bar{\rho}\tilde{\xi})}{\partial t} + \frac{\partial(\bar{\rho}\tilde{u}_k\tilde{\xi})}{\partial x_k} = \frac{\partial}{\partial x_k} \left( \overline{\rho D \frac{\partial \xi}{\partial x_k}} \right) - \frac{\partial(\bar{\rho}\tilde{u}_k''\tilde{\xi}'')}{\partial x_k}.$$

For a non-reacting scalar the gradient assumption can be used for the last term on the right hand-side (see [16]), so  $\tilde{u}_k''\tilde{\xi}'' = -D_t \frac{\partial \xi}{\partial x_k}$ . In a turbulent flow the turbulent diffusion coefficient  $D_t$  is much larger than molecular diffusivity, so the latter is usually neglected.

As we shall see later, the second moment of the mixture fraction,  $\tilde{\xi}''^2$ , is a parameter in the assumed probability density function (PDF), so we must solve an additional equation for its temporal evolution (Eq. (3.3), [5, 17]).

$$(3.3) \quad \frac{\partial(\bar{\rho}\tilde{\xi}''^2)}{\partial t} + \frac{\partial(\bar{\rho}\tilde{u}_k\tilde{\xi}''^2)}{\partial x_k} = \frac{\partial}{\partial x_k} \left( \bar{\rho} \frac{\nu_{\text{turb}}}{Sc} \frac{\partial \xi''^2}{\partial x_k} \right) + 2\bar{\rho} \frac{\nu_{\text{turb}}}{Sc} \left( \frac{\partial \tilde{\xi}}{\partial x_k} \right)^2 - C_d \bar{\rho} \frac{\tilde{\epsilon}}{\tilde{\rho}} \tilde{\xi}''^2.$$

The mean values of the reacting scalars (mass fractions of all species) can be calculated from Eq. (3.4) using the presumed shape of the PDF of the mixture fraction,  $P(\xi)$ , and integrating over the whole mixture fraction space,

$$(3.4) \quad \tilde{Y}_\alpha = \int_0^1 Y_\alpha(\xi) \tilde{P}(\xi) d\xi \quad .$$

The shape of  $\tilde{P}(\xi)$  is an empirical result of many experiments (cf. [12]). In the numerical simulations of turbulent combustion mainly two kinds of PDFs are used: the clipped Gaussian function or a beta function, both parametrised by the mean value of the mixture fraction (obtained by solving Eq. (3.2) with a CFD code) and by the root mean square of the fluctuation of mixture fraction (obtained by solving Eq. (3.3)). Alternatively, the whole set of equations for the reacting species should be solved directly, which is a lot slower and less convenient. An example of such computations for simplified reactions in a developing mixing layer was given in [20].

### 3.2. Laminar flamelet

Combustion takes place when two conditions are fulfilled. Firstly, the value of the mixture fraction should be close to stoichiometric, which ensures the appropriate proportion of fuel and oxidiser. Secondly, there should be a large gradient of the mixture fraction, which distinguishes the case when fresh fuel is mixing with oxidiser from the case when fuel and oxidiser are already burnt [4]. Often

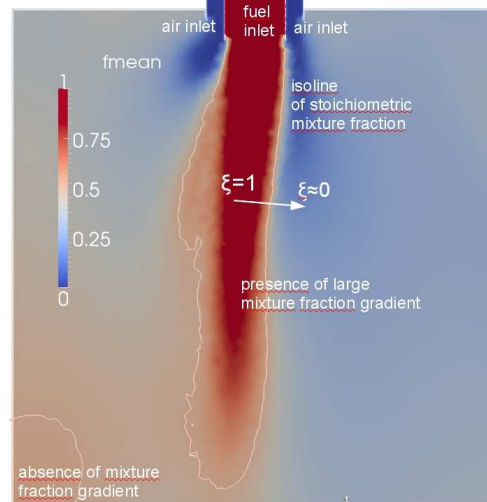


FIG. 2. Typical mixture fraction distribution near the inlets.

such zones (flamelets) are considerably thinner than the smallest characteristic length scale of turbulence (the Kolmogorov scale) and can be treated as a wrinkled sheet of constant, stoichiometric value of the mixture fraction [15]. Locally it is possible to introduce the coordinate system with two coordinates parallel to the isosurfaces of the mixture fraction (see Fig. 2) and with mixture fraction as the transversal coordinate.

Peters [16] reviewed the formal introduction of this coordinate transformation and derived the equations for the mass fractions of all species (Eq. (3.5)) and for temperature (Eq. (3.6)). The main processes in the ‘mixture fraction space’ are diffusion and chemical reactions. The influence of the fluid flow on mixing is accounted for by considering the quantity called scalar dissipation rate,  $N = 2D\nabla\xi \cdot \nabla\xi$ , which may be interpreted as the inverse of the characteristic time scale of diffusion [3].

$$(3.5) \quad \frac{1}{2}\rho N(\xi) \frac{\partial^2 Y_\alpha}{\partial \xi^2} + \omega_\alpha = 0,$$

$$(3.6) \quad \frac{1}{2}\rho N(\xi) \frac{\partial^2 T}{\partial \xi^2} + \omega_T = 0.$$

Boundary conditions for these equations are like those for the counter-flowing jets of fuel and oxidiser with a stagnation point.

The great advantage of the methods based on tabulated chemistry, like the laminar flamelet method, is the possibility of doing all calculations of the chemical reactions once, before running the fluid-mechanical simulations. The flamelet

library built in such a way consists of the solutions of Eqs. (3.5) and (3.6) depending on the values of the mixture fraction and the scalar dissipation rate. Both these quantities, and also the variations of the mixture fraction that are necessary for the beta-function PDF, are computed in the CFD code.

## 4. Results and discussion

### 4.1. Flamelet properties

We calculated the flamelet library for combustion of the biomass syngases produced from wood chips and from turkey feathers (see Table 1). Two values of temperature of the inlet syngases are considered, the typical value of 1000 K and the low value of 800 K. In Fig. 3 we plot the maximum temperature observed within the reaction layer as a function of the scalar dissipation rate for the four syngases (two types of gasified biomass and two inlet temperatures). The results depend strongly on the syngas calorific values. The wood syngases sustain the combustion even for high values of the scalar dissipation rate (higher than

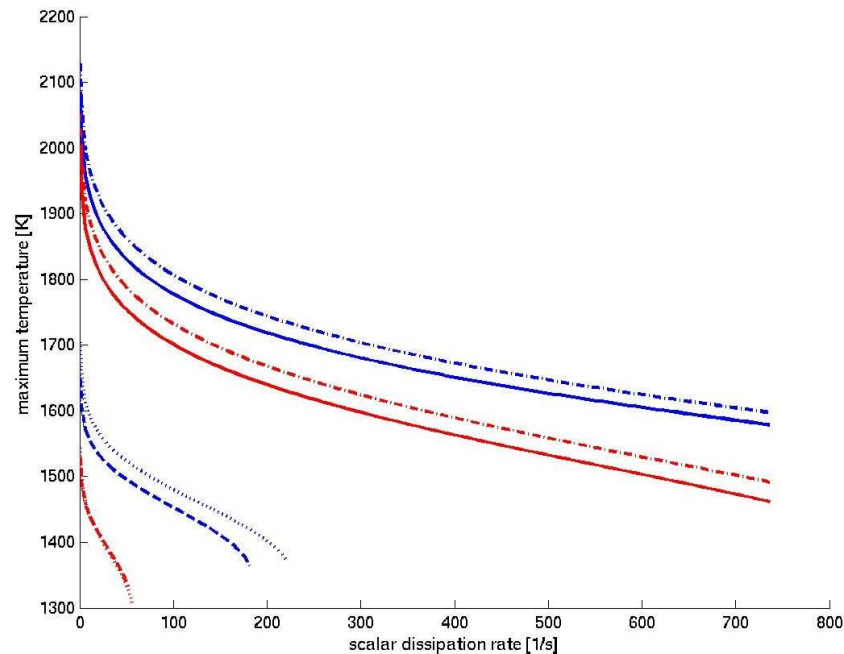


FIG. 3. Dependence of syngas combustion on the scalar dissipation rate for different kinds of syngases. Solid lines – wood syngas (WS1), dashed lines – wood syngas (WG2), dotted lines – feathers syngas (FS1), dash-dotted lines – feather syngas (FS2). The initial temperatures of the syngases are marked with colour: blue lines – initial temperature equal 1000 K; red lines – initial temperature equal 800 K.

200 s<sup>-1</sup>) while the syngases produced from feathers are prone to extinction for such values. Increasing of the initial temperatures of the feathers syngases helps to maintain combustion for lower values of the scalar dissipation rate. According to our simulations the scalar dissipation rate does not exceed 50 s<sup>-1</sup>. Hence, even for the gas obtained from the gasification of feathers extinctions do not occur spontaneously. From the flamelet chemistry it follows that when temperature of the fuel exceeds 1000 K the process is stable and no extinctions occur. This is confirmed in working gasification plants.

The flamelet library tabulates the dependence of temperature and of the mass fractions of the species on the mixture fraction. In Fig. 4 the temperatures in the mixture fraction space are presented for the scalar dissipation rate equal 0.01 s<sup>-1</sup>.

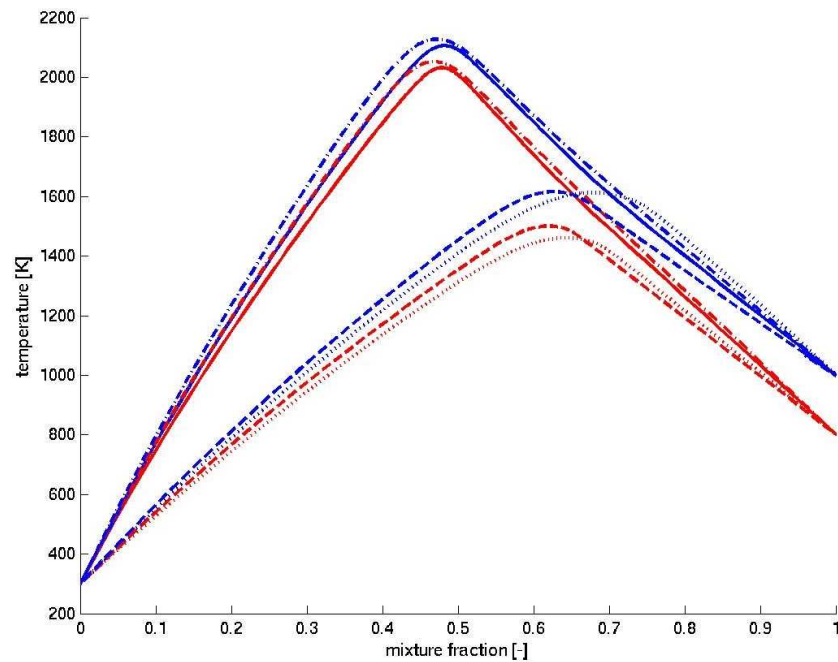


FIG. 4. Solutions of the flamelet equations show the dependence of temperature on the mixture fraction. Solid lines – wood syngas (WS1), dashed lines – wood syngas (WG2); dotted lines – feathers syngas (FS1), dash-dotted lines – feather syngas (FS2). The initial temperatures of the syngases are marked with colour: blue lines - initial temperature equal 1000 K; red lines – initial temperature equal 800 K.

The profiles vary in maximum temperatures of reaction from around 1500 K for the syngas from feathers at initial temperature 800 K, through 1600 K when the initial temperature is 1000 K, to 2000 K for the wood-chip syngas at initial temperature 800 K. For hot wood-chip syngas this value increases to 2100 K.

The dependence of carbon monoxide, nitric oxide and nitrogen dioxide mass

fraction on the mixture fraction is plotted in Fig. 5. For NO, whose production is correlated with temperature, the values for wood-chip syngases largely exceed those for the feather-derived fuels (see Fig. 5b). Strong dependence on the initial temperature is also visible. The higher is the initial temperature, the higher the NO mass fraction. In contrast the production of NO<sub>2</sub> for both kinds of syngas is similar and low (see Fig. 5c).

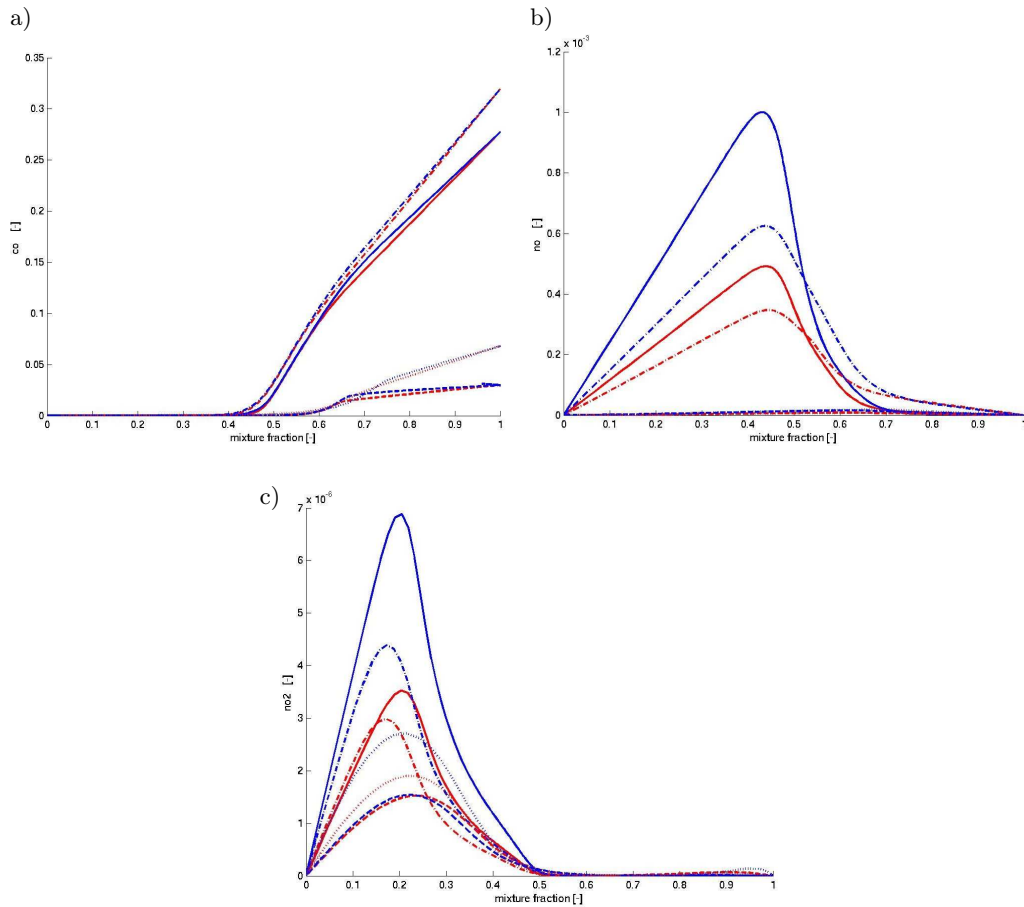


FIG. 5. Solutions of the flamelet equations for the scalar dissipation rate of  $0.01 \text{ s}^{-1}$ . The panels show the dependence of (a) carbon monoxide, (b) nitric oxide and (c) nitrogen dioxide concentrations on the mixture fraction. Solid lines – wood syngas (WS1), dashed lines – wood syngas (WG2), dotted lines – feathers syngas (FS1), dash-dotted lines – feather syngas (FS2). The initial temperature of syngases is marked with colour: blue line – initial temperature equal 1000 K; red lines – initial temperature equal 800 K.

#### 4.2. Combustion

The results are obtained using the steady-state and transient pressure-based Fluent solver. Among the simulated processes are turbulent flows, energy transfer, radiation and non-premixed combustion. The details of the fluent setup are listed in Table 3. The simulations were done on two meshes: fine mesh with  $10^6$  nodes and coarse mesh with  $0.5 \cdot 10^6$  nodes.

**Table 3. Summary of the fluent setup for the simulations of turbulent combustion.**

Models	
Turbulence	Realizable $k - \epsilon$
Radiation	P1
Non-premixed combustion	Steady Flamelet
Solver	Steady-state Pressure based

The steady-state simulations were performed first to reproduce the main features of the combustion process. Even those steady simulations are in good agreement with the observations in the working industrial burner. The length of the jets is consistent with observations – they reach down, roughly, to the middle of the combustion chamber (see Fig. 6). Also, the simulations in all cases predict the presence of an updraft near the wall of the chamber. In the real, working combustion chamber the effect of this updraft is clearly visible in the observed pattern formed by the solid particles deposited on the wall.

Visual observations, as well as the analysis of the high-speed camera recording, show the combustion process to be unsteady. The time dependence of the flow and the effects of unsteadiness cannot be captured by the steady-state (RANS) simulations. In particular we are not able to predict any time-dependent phenomena, like oscillations of the length of the jet or jet precession. We have analysed these effects of unsteadiness using both Unsteady RANS simulations and Large Eddy Simulations (LES). The jet precession, as we show in Fig. 8, has been observed. The unsteady, oscillatory character of the solution explains the differences between the steady-state solutions presented in panels a) and b) in Figs. 6 and 7. The steady-state solution poorly converges and is sensitive to the numerical details, such as even small changes in the mesh size, because it is, presumably, unstable and would have the tendency to become oscillatory if not the steadiness imposed by the RANS method. The details of the LES results are presented and compared elsewhere [13].

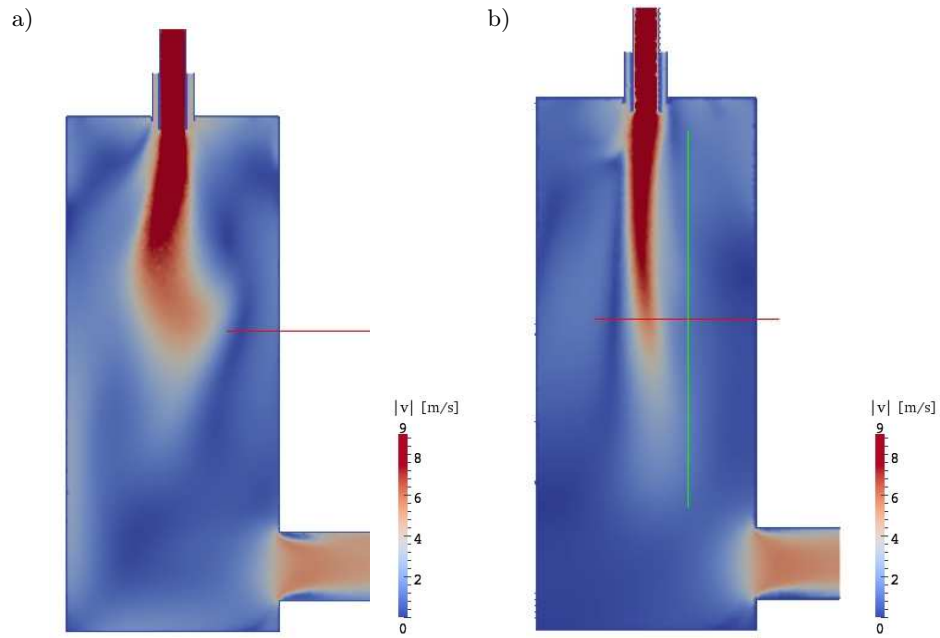


FIG. 6. The steady-state results. Colour map of the velocity magnitude in the  $x$ - $z$  plane sections: a) fine mesh ( $10^6$  nodes), b) coarse mesh ( $0.5 \cdot 10^6$  nodes).

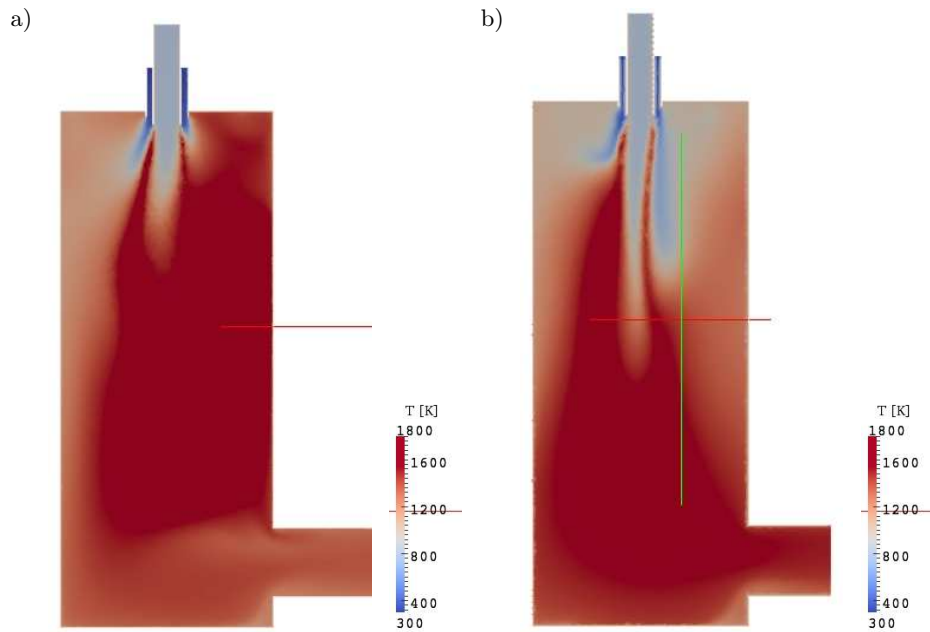


FIG. 7. Steady-state results of the combustion simulations computed with Fluent. Colour maps of temperature in the  $x$ - $z$  plane sections: a) fine mesh ( $10^6$  nodes), b) coarse mesh ( $0.5 \cdot 10^6$  nodes).

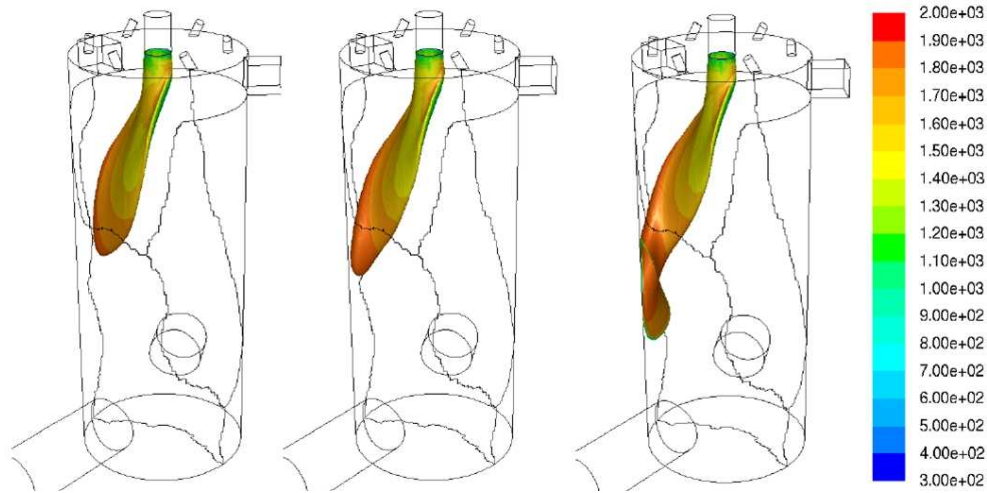


FIG. 8. The results of the Unsteady RANS. The isosurface of the stoichiometric value of mixture fraction coloured by temperature. The time interval between the snapshots is equal 0.6 s.

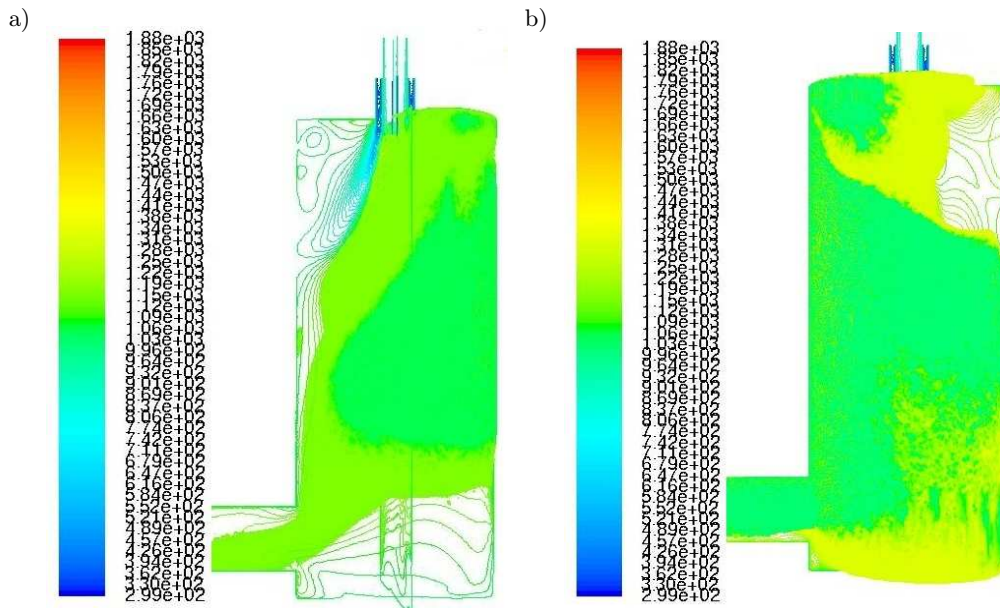


FIG. 9. The results of the Unsteady RANS. The fraction of the combustion chamber volume where temperature exceeds  $850\text{ }^{\circ}\text{C}$  at two times.

The main result of this work, which is observed for both steady and unsteady cases, is that the temperature in almost entire volume of the combustion chamber is higher than the required  $850\text{ }^{\circ}\text{C}$ . In Fig. 9 we show, at two times, the fraction of

the combustion chamber volume where temperature is higher than required. The precession of the marked volume reflects the precession of the jet. The average temperature at the outlet is  $980^{\circ}\text{C}$  with standard deviation of  $50^{\circ}\text{C}$ . This is in good agreement with the temperature at the outlet of the combustion chamber measured in the feathers gasification plant in Olsztyn (see Fig. 10).

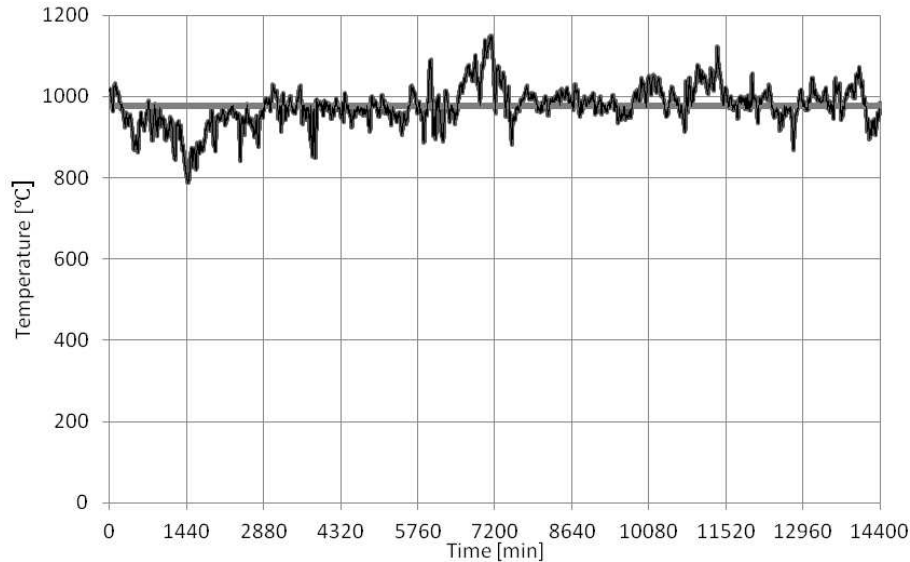


FIG. 10. The temperature at the outlet of the combustion chamber where the syngas from feathers is burnt. The data for 10 days (1.03.2011–10.03.2011) are plotted. The average value (grey line) is close to  $1000^{\circ}\text{C}$ . The standard deviation is smaller than  $50^{\circ}\text{C}$ .

## 5. Conclusions

In the present paper we have shown that biomass syngas, whose popularity as an energy source increases, is a valuable fuel useful for heat production. The fuel supplied to the combustion chamber is hot, which is rather unusual compared with other combustion processes. Therefore, the properties of the flame are not readily and have to be calculated and tabulated. Such special conditions enable burning the low-calorific biomass syngas without additional oil burner and with almost no post-processing of the flue gases. This is possible even for low-calorific biomass syngas due to the fact that almost half of the total energy of the gas is in the form of heat. The rest of the energy, contained mostly in hydrogen, carbon monoxide and methane, is sufficient to sustain combustion. The process is practical in industrial heat production and economically viable even for low-calorific syngas produced from feathers [7, 14], where combustible gases comprise less than 10% of the mass of the syngas.

## Acknowledgements

Part of this work was supported by the strategic program of scientific research and experimental development of the Polish National Centre for Research and Development: “Advanced Technologies for Energy Generation”; Task 4. “Elaboration of Integrated Technologies for the Production of Fuels and Energy from Biomass as well as from Agricultural and other Waste Materials”. One of us (KK) acknowledges financial support from the Foundation for Polish Science Programme VENTURES. Numerical computations were performed in the Interdisciplinary Centre for Computational and Mathematical Modelling (ICM), University of Warsaw, grant number G34-8. KB acknowledges the support of the COST Action MP0806.

## References

1. Council directive 75/442/eec on waste (changed by directive 91/156/ewg and directive 91/689/ewg).
2. Directives 89/429/ewg, 94/67/we and 2000/76/we.
3. R.W. BILGER, *Some aspects of scalar dissipation*, Flow, turbulence and combustion, **72**, 2, 93–114, 2004.
4. R.W. BILGER, S.B. POPE, K.N.C. BRAY, J.F. DRISCOLL, *Paradigms in turbulent combustion research*, Proceedings of the Combustion Institute, **30**, 1, 21–42, 2005.
5. R.S. CANT, E. MASTORAKOS *An Introduction to Turbulent Reacting Flows*, Imperial College Press, 2008.
6. A. CUOCI, A. FRASSOLDATI, G. BUZZI FERRARIS, T. FARAVELLI, E. RANZI, *The ignition, combustion and flame structure of carbon monoxide/hydrogen mixtures. Note 2: Fluid dynamics and kinetic aspects of syngas combustion*, Int. J. Hydrogen Energy, **32**, 15, 3486–3500, 2007.
7. M. DUDYŃSKI, K. KWIATKOWSKI, K. BAJER, *From feathers to syngas – technologies and devices*, Waste Management, **32**, 4, 685–691, 2012.
8. M. DUDYŃSKI, *Rights of protection no. (21) 385282: Sposób i urządzenie do zgazowania odpadów organicznych*, Technical report, Modern Technologies and Filtration Sp. z o.o., 2008.
9. A. FRASSOLDATI, T. FARAVELLI, E. RANZI, *The ignition, combustion and flame structure of carbon monoxide/hydrogen mixtures. Note 1: Detailed kinetic modeling of syngas combustion also in presence of nitrogen compounds*, Int. J. Hydrogen Energy, **32**, 15, 3471–3485, 2007.
10. C. HIGMAN, M. VAN DER BURGT, *Gasification*, 2nd ed., Gulf Professional Publishing, 2008.
11. D.L. KLASS, *Biomass for Renewable Energy, Fuels, and Chemicals*, Academic Press, 1998.
12. A.Y. KLIMENKO, R.W. BILGER, *Conditional moment closure for turbulent combustion*, Progress in Energy and Combustion Science, **25**, 6, 595 – 687, 1999.

- 
13. K. KWIATKOWSKI, D. JASIŃSKI, K. BAJER, *Numerical simulations of industrial-scale combustion chamber – LES versus Rans*, J. of Physics: Conference Series, **318**, 092009, 2011.
  14. K. KWIATKOWSKI, J. KRZYSZTOFORSKI, K. BAJER, M. DUDYŃSKI, *Gasification of feathers for energy production – a case study*, Proceedings of 20th European Biomass Conference and Exhibition, Milan, 1858–1862, 2012.
  15. N. PETERS, *Laminar diffusion flamelet models in non-premixed turbulent combustion*, Progress in Energy and Combustion Science, **10**, 3, 319 – 339, 1984.
  16. N. PETERS, *Turbulent Combustion*, Cambridge University Press, 2000.
  17. T. POINSOT, D. VEYNANTE, *Theoretical and Numerical Combustion*, R.T. Edwards, Inc., 2005.
  18. P. QUAACK, H. KNOEF, H. STASSEN, *Energy from biomass. A review of combustion and gasification technologies*, World Bank Technical Paper, **422**, The World Bank, 1999.
  19. G.P. SMITH, D.M. GOLDEN, M. FRENKLACH, N.W. MORIARTY, B. EITENEER, M. GOLDENBERG, C.T. BOWMAN, R.K. HANSON, S. SONG, W.C. GARDINER, V.V. LISSIANSKI, Z. QIN, [http://www.me.berkeley.edu/gri\\_mech/](http://www.me.berkeley.edu/gri_mech/).
  20. K. WĘDOŁOWSKI, K. KWIATKOWSKI, K. BAJER, *Analysis and modelling of the effective reaction rate in a developing mixing layer*, Journal of Physics: Conference Series, **318**, 092026, 2011.

Received February 17, 2011; revised version March 7, 2012.

---